Thermochemical Nonequilibrium in an Argon Constricted Arc Plasma

K. J. CLARK* AND F. P. INCROPERA†
Purdue University, West Lafayette, Ind.

Theme

THIS paper presents the results of a theoretical investigation of thermochemical nonequilibrium in an argon arc plasma. A multifluid model is used to describe the nonequilibrium plasma, and the resulting numerical solutions are compared with both existing experimental data and equilibrium solutions. In addition, a parametric study is performed to determine the spatial extent of the nonequilibrium condition as a function of arc operating variables, and the effects of collision-cross-section and wall-temperature uncertainties on the predictions are ascertained.

Contents

Although nonequilibrium in arc plasmas has been observed in a number of recent experimental investigations, comparatively little effort has been devoted to a rigorous theoretical analysis of this phenomenon. Hence, the present investigation is concerned with the formulation and solution of a model which is physically complete in terms of both governing equations and boundary conditions.

The following definition of thermochemical nonequilibrium is appropriate for an argon arc plasma and provides the basis for the physical model used in this study: two distinct kinetic temperatures are defined, corresponding to the electrons and the heavy particles, and the Saha equation is insufficient to determine the local composition.

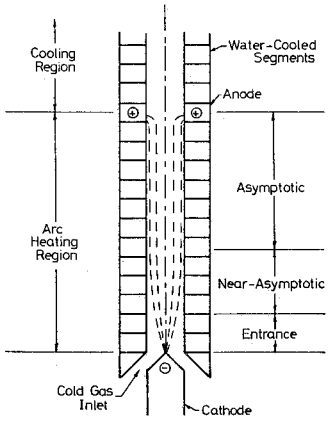

Fig. 1 Schematic diagram of a constricted arc plasma.

Figure 1 presents a schematic diagram of the constricted arc and delineates the near-asymptotic and asymptotic regions which are of interest. The near-asymptotic region is defined as that portion of the arc plasma in which the radial electric current component and axial transport phenomena are negligible. The thermal and hydrodynamic flowfields are coupled, however, and are governed by boundary-layer-type equations. The asymptotic region is characterized by a fully developed thermal condition and negligible radial convective velocities. It follows that the thermal and hydrodynamic flowfields are decoupled in this region.

Eight dependent variables are used to specify the nonequilibrium condition in the near-asymptotic region: electron and heavy-particle temperatures (T_e, T_h), electron and atom number densities (n_e, n_A), axial and radial convective velocities (u, v), pressure (p), and axial electric field intensity (E_z). The eight associated governing equations are electron continuity and energy, heavy-particle energy, global continuity and axial momentum, perfect gas thermal equation of state, and integral expressions which dictate the conservation of electric current and total mass flowrate. Because of the aforementioned decoupling in the asymptotic region, five dependent variables are sufficient for this region: T_e, T_h, n_e, n_A, and E_z; and the global continuity equation, global axial momentum equation, and the total mass flowrate integral equation are no longer necessary. The required boundary conditions are based upon symmetry at the duct centerline, the assumption of thermal equilibration and zero slip between the heavy-particle subgas and the duct wall, and the presumed existence of a collisionless electrostatic sheath model which describes the interaction of the electron subgas with the wall. The sheath model utilizes reflection coefficients to account for variable wall catalycity effects.

Laminar, steady, axisymmetric flow with negligible viscous dissipation is assumed. In addition, the plasma is assumed to be quasi-neutral and comprised of only free electrons, single ions, and neutral atoms. The transport phenomena considered are electron and heavy-particle subgas thermal conduction, ambipolar concentration and thermal diffusion, viscous shear, and electron current drift. Inelastic collisions and radiative processes included in the model are electron-atom and atom-atom collisional excitation, deexcitation, ionization, and recombination; radiative recombination; spontaneous radiative deexcitation; and bremsstrahlung. Simple models are developed to treat each of these processes. The aforementioned equations and boundary conditions comprise the most rigorous and complete physical model presently available for the laminar arc plasma.

The asymptotic region is of primary interest since the only reliable experimental data pertains to this region. A finite-difference iteration scheme was devised to solve the associated governing equations subject to the sheath boundary conditions. The method requires an accurate initial estimate of the actual solution, which is obtained by solving the near-asymptotic equations up to the asymptotic region, subject to fixed wall conditions for the electron subgas. An explicit finite-difference technique was developed to solve the near-asymptotic equations.

Nonequilibrium predictions are compared with available experimental data for an argon arc with duct radius $r_w = 0.5$ cm, $p = 1$ atm, and an arc current range $35 \leq I < 400$ amp. These predictions agree with data to within the experimental uncertainties: E_z, $\pm 3\%$; total wall heat flux (q_w), $\pm 6\%$; fraction of q_w due to radiation (q_{rad}/q_w), $\pm 10\%$; and $T_e(r)$, $\pm 2.5\%$. Furthermore,

Presented as Paper 71-593 at the AIAA 4th Fluid and Plasma Dynamics Conference, Palo Alto, Calif., June 21–23, 1971; submitted June 21, 1971; synoptic received June 21, 1971. Full paper available from AIAA. Price: AIAA members, $1.50; nonmembers, $2.00. Microfiche, $1.00. **Order must be accompanied by remittance.**

* Graduate Research Assistant, School of Mechanical Engineering; presently Staff Engineer, Acurex Corporation, Mountain View, Calif. Associate Member AIAA.

† Associate Professor, School of Mechanical Engineering, Purdue University, West Lafayette, Ind. Member AIAA.

for the entire range of wall catalycity, $0.0 \leqslant \chi = \beta \leqslant 0.99$, the quantities E_z, q_w, and q_{rad}/q_w vary by no more than 4%. (Note: β and χ are the fraction of electrons and ions, respectively, striking the wall which are reflected.) Variations in χ and β have no effect upon $T_e(0)$ and $n_e(0)$, but $T_e(r_w)$ increases by roughly 20% and $n_e(r_w)$ decreases by a factor of 50 when χ and β are varied from 0.99 to 0.0.

Relative to the experimental data, the nonequilibrium predictions offer a substantial improvement over the available equilibrium predictions. This is evidenced by the following maximum discrepancies between the data and the corresponding equilibrium predictions: E_z, $\pm 15\%$; q_w, $\pm 20\%$; q_{rad}/q_w, $+100\%$; $T_e(0)$, $+10\%$; and $T_e(r_w)$, -900%.

In the parametric study utilizing the nonequilibrium model, solutions are obtained for a wide range of arc operating conditions: $35 \leqslant I \leqslant 400$ amp, $0.2 \leqslant p \leqslant 10.0$ atm, $0.3 \leqslant r_w \leqslant 0.9$ cm. It is found that for certain values of I, p, and r_w the temperatures T_e and T_h are essentially equal in the arc core, indicating the existence of thermal equilibrium in this region. Under the same conditions, the actual nonequilibrium electron number density n_e, and that computed from the Saha equation evaluated at the local value of T_e, $n_e^*(T_e)$, or the local value of T_h, $n_e^*(T_h)$, are all in close agreement, indicating the existence of chemical equilibrium. However, for all conditions T_e and T_h and n_e, $n_e^*(T_e)$, and $n_e^*(T_h)$ diverge as the wall is approached. Typically, T_e remains elevated at 7000–10,000°K, and n_e is many orders of magnitude greater than $n_e^*(T_h)$ in the vicinity of the wall. Also, the radial position for the onset of thermal nonequilibrium is found to coincide with that for the onset of ionization nonequilibrium. Finally, for certain values of I, p, and r_w this divergence is found to occur at the duct centerline; that is, the entire arc is in a condition of thermochemical nonequilibrium. When nonequilibrium prevails at the duct centerline, the condition $T_e > T_h$ occurs, as in the vicinity of the wall, but n_e is less than either $n_e^*(T_e)$ or $n_e^*(T_h)$, in contrast to the condition at the wall.

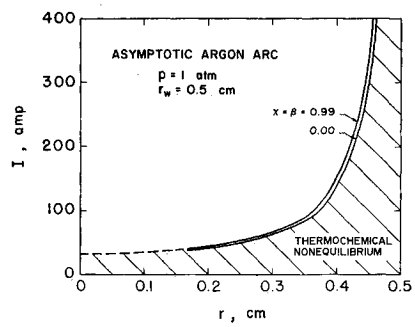

Fig. 2 Radial location of departure from local thermodynamic equilibrium vs arc current.

Assuming the condition $T_e - T_h \geqslant 300$°K to represent the onset of thermochemical nonequilibrium, Fig. 2 shows the departure from equilibrium as a function of I, for fixed p and r_w. It is apparent that this departure point moves radially inward with decreasing I. In addition, the departure is found to shift towards the duct centerline with decreasing p (fixed I and r_w) and increasing r_w (fixed I and p).

All of the aforementioned nonequilibrium predictions are obtained assuming the duct wall temperature (T_w) to be 1000°K. For a $\pm 25\%$ variation in T_w the following effects on predicted quantities for the 100 amp arc are typical: $E_w \mp 0.25\%$; $T_e(0)$, $\mp 0.04\%$; $T_e(r_w)$, $\pm 0.75\%$; $n_e(0)$, $\mp 0.3\%$; $n_e(r_w)$, $+16\%$, -9%. Each of the cross sections used in the model is also varied separately to its maximum uncertainty, with the following perturbations resulting in the predicted quantities: E_z, -8.1%; $T_e(0)$, -1.6%; $T_e(r_w)$, $+1.9\%$; $n_e(0)$, -13.7%; $n_e(r_w)$, $+9.6\%$. The relatively small effects of these uncertainties indicate that predictions of engineering accuracy can be obtained despite the relatively high uncertainties in T_w and several of the cross sections.